

# Hierarchy in the halogen activation during surface-promoted Ullmann coupling

Néstor Merino-Díez,<sup>[a, b, c]</sup> Alejandro Pérez Paz,<sup>[d]</sup> Jingcheng Li,<sup>[b]</sup> Manuel Vilas-Varela,<sup>[e]</sup> James Lawrence,<sup>[a, c]</sup> Mohammed S. G. Mohammed,<sup>[a, c]</sup> Alejandro Berdonces-Layunta,<sup>[a, c]</sup> Ana Barragán,<sup>[c, f]</sup> J. Ignacio Pascual,<sup>[b, g]</sup> Jorge Lobo-Checa,<sup>[h]</sup> Diego Peña,<sup>[e]</sup> and Dimas G. de Oteyza<sup>\*[a, c, g]</sup>

**Abstract:** Within the collection of surface-supported reactions currently accessible for the production of extended molecular nanostructures under ultra-high vacuum, Ullmann coupling has been the most successful in the controlled formation of covalent single C-C bonds. Particularly advanced control of this synthetic tool has been obtained by means of hierarchical reactivity, commonly achieved by the use of different halogen atoms that consequently display distinct activation temperatures. Here we report on the site-selective reactivity of certain carbon-halogen bonds. We use precursor molecules halogenated with bromine atoms at two non-equivalent carbon atoms and found that the Ullmann coupling occurs on Au(111) with a remarkable predilection for one of the positions. Experimental evidence is provided by means of scanning tunneling microscopy and a rationalized understanding of the observed preference is obtained from density functional theory calculations.

## Introduction

A continuous boost of computing power is at the core of current technology roadmaps. So far, the most promising approach in this

pursuit involves the maximization of the number of electronic components per integrated circuit. With silicon-based technology reaching scaled-down saturation, single molecules displaying basic electronic functionalities (rectifiers, switches...) are among the most promising alternatives for the substitution of current electronic components<sup>[1]</sup>. However, an effective manufacturing of molecular electronics requires a precise control of the structure not only within the functional elements but also of their respective linkage. In this context, on-surface synthesis represents a promising platform for the implementation of molecular electronics<sup>[2]</sup>. Besides expanding the synthetic routes available for creating different forefront materials, it results in designed materials that readily feature suitable two-dimensional structure for their subsequent implementation into planar integrated circuits<sup>[3]</sup>.

Aiming at their successful integration in future devices, such functional materials require mechanical robustness and high electron mobility, for which covalent bonds stand out when compared to weaker interactions<sup>[4]</sup>. Inspired by conventional wet-chemistry, numerous reactions yielding C-C bond formation have already been achieved on surfaces, including Sonogashira coupling<sup>[5]</sup>, aldehyde-amine coupling<sup>[6]</sup> or Glaser coupling<sup>[7]</sup> among others<sup>[8]</sup>. Nevertheless amid this collection of C-C generating reactions, Ullmann coupling (UC), in which two aryl halides are coupled on a catalytic surface (such as the facets of commonly used coinage metals) to form a biaryl molecule, represents the most widespread one to date<sup>[9]</sup>. A milestone in the development of UC as the leading on-surface synthesis reaction scheme was set by Grill and coworkers<sup>[10]</sup>, who demonstrated how the morphology and dimensionality of molecular networks can be precisely tuned by adding halogen atoms at different linking sites within the same precursor backbone. Ever since, UC has been tested on a large number of different substrates and aromatic precursors<sup>[11]</sup>, highlighting its versatility for the on-surface formation of different low-dimensional nanostructures.

Advanced control of on-surface synthesis protocols has been obtained through hierarchical processes<sup>[12]</sup>. That is, controlled sequences of reactions which promote the correct step-by-step connection of molecules in the formation of complex molecular structures. With UC, this hierarchy can be achieved by functionalizing the carbon backbone with different halogens, since each of them features different energy barriers for the scission of its carbon-halogen bond<sup>[13]</sup>. In this work we show how, even when using the same halogens, a selective activation of specific C-Br bonds can be obtained by different means, namely depending on their location within the same aromatic precursor. Our combined scanning tunneling microscopy (STM) and density functional theory (DFT) results reveal that this site-selectivity is driven by the substrate and the X shape conformation of the precursor. At the

- [a] N. Merino-Díez, Dr. J. Lawrence, M. S. G. Mohammed, A. Berdonces-Layunta, Dr. Dimas G. de Oteyza  
Donostia International Physics Center (DIPC)  
20018 San Sebastián, Spain  
E-mail: d\_g\_oteyza@ehu.eus
- [b] N. Merino-Díez, Dr. J. Li, Dr. J. I. Pascual  
CIC nanoGUNE, nanoscience cooperative research center  
20018 San Sebastián, Spain
- [c] N. Merino-Díez, Dr. J. Lawrence, M. S. G. Mohammed, A. Berdonces-Layunta, A. Barragán, Dr. Dimas G. de Oteyza  
Centro de Física de Materiales – MPC, CISC-UPV/EHU  
20018 San Sebastián, Spain
- [d] Dr. A. Pérez Paz  
School of Physical Sciences and Nanotechnology, Yachay Tech University  
100119 Urcuquí, Ecuador
- [e] M. Vilas-Varela, Dr. D. Peña  
CIQUS, Centro Singular de Investigación en Química Biolóxica e Materiais Moleculares  
15705 Santiago de Compostela, Spain
- [f] A. Barragán  
Departamento de Física de Materiales, Universidad del País Vasco (UPV/EHU)  
20018 San Sebastián, Spain
- [g] Dr. J. I. Pascual, Dr. D. G. de Oteyza  
Ikerbasque, Basque Foundation for Science  
48013 Bilbao, Spain
- [h] Dr. Jorge Lobo-Checa  
Instituto de Ciencia de Materiales de Aragón, CSIC-Universidad de Zaragoza 50009 Zaragoza

preferred adsorption configuration of the precursor, the halogens display different distances to the metal surface, which leads to a strongly modulated catalytic effect of the substrate for each C-Br bond.

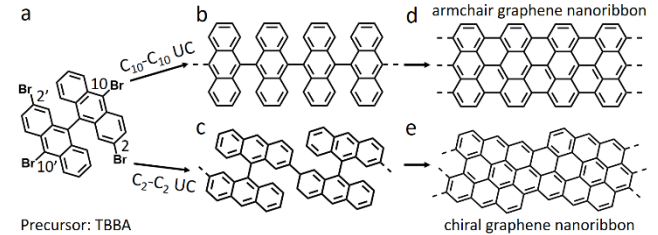
## Results and Discussion

In this experiment we make use of 2,2',10,10'-tetrabromo-9,9'-bianthracene (TBBA, Fig. 1a, see supporting information for the synthesis and characterization of this molecule). The reactivity of similar di-brominated bianthracyne (DBBA) precursors, having halogen atoms located either at 10 and 10' or at 2 and 2' positions, has been previously reported for different coinage metal surfaces<sup>[14]</sup>. When bromine atoms are excised preferentially at positions 2 and 2', UC governs the synthetic process and renders, after subsequent thermal cyclodehydrogenation (CDH), chiral graphene nanoribbons (chGNRs) on Au(111), Ag(111) and Cu(111) (Fig. 1e)<sup>[14]</sup>. Similarly, when bromine atoms are excised at positions 10 and 10', armchair GNRs are obtained on Au(111) and Ag(111)<sup>[14]</sup> (Fig. 1d) through UC and CDH. However, the coupling selectivity given by the halogen excision is overruled by the substrate's catalytic effect on Cu(111). In this case, new radicals are created via dehydrogenation at C<sub>2</sub> positions, which ultimately determine the polymerization motif and yield chGNRs upon CDH<sup>[14]</sup>. The fact that the same results are obtained even with non-halogenated bianthracyne precursors demonstrate that this coupling mechanism is fully independent of whether radicals are present at 10,10' positions or not<sup>[15]</sup>. These findings highlight the complex competition in the determination of the reaction mechanism between the halogen position within the aromatic skeleton and the specific interactions with the substrate. Here, we employ TBBA precursors (Fig. 1a) on Au(111) in an attempt to specifically address this interplay.

After TBBA deposition, UC is thermally-induced at ~450 K and TBBA precursors form bianthracyne polymers. Figure 2 shows different scale STM images of this phase. As also observed with either type of DBBA reactants, the polymers appear aggregated into islands, indicating the presence of attractive intermolecular forces. These polymers are seen as a series of zigzagging lobes

corresponding to the up-pointing termini of anthracene subunits. The latter arrange in an alternatingly tilted non-planar configuration to minimize the steric hindrance exerted by the neighbouring hydrogen atoms. Because this zigzag-display is shared by both armchair and chiral GNRs<sup>[14]</sup>, an unambiguous determination of the polymer structure is not straightforward at this point.

**Figure 1.** Possible synthetic routes expected in this experiment from (a) TBBA precursor. (b) Debromination and C<sub>10</sub>-C<sub>10</sub> Ullmann coupling (UC) followed by



cyclodehydrogenation (CDH) leads to (d) armchair GNRs formation. (c) Debromination and C<sub>2</sub>-C<sub>2</sub> UC (c) followed by CDH leads to (e) chiral GNRs, the preferred pathway here. Note that primed position x' is chemically equivalent to the corresponding unprimed position x and either would yield the same GNR.

Figure 2 also reveals the presence of a disordered network surrounding the polymeric islands and spreading over the remaining Au(111) surface. A closer look reveals that this web consists of single circular adsorbates arranged either in line or in a zigzag manner (Fig. S3). Similar networks have been observed for submonolayer coverages of halogens on Au(111)<sup>[16]</sup>, as well as with other GNR precursors with a large stoichiometric halogen ratio,<sup>[17]</sup> which leads us to the conclusion that these adsorbates are bromine atoms. This kind of networks has not been observed in polymers formed from similar di-brominated precursors because the halogens are preferentially placed underneath the up-pointing anthracene ends, "hidden" from the scanning probe<sup>[18]</sup>. The observed Br network is thus assigned to the additional Br atoms as we change from dibrominated to tetrabrominated reactants, which can no longer be incorporated below the polymers. This finding underlines that both 2,2' as well as 10,10' positions are dehalogenated at this stage.

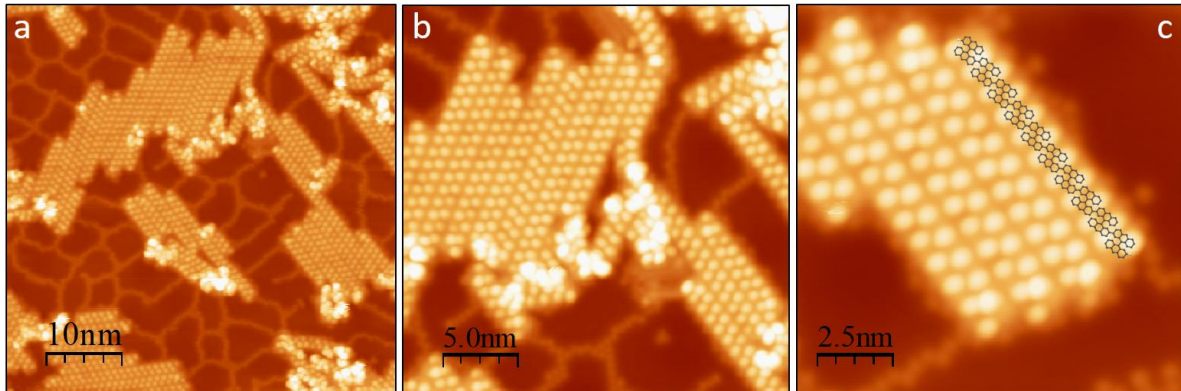


**Figure 2.** STM images of polymeric phase. (a) 50 nm<sup>2</sup> (U = 1.4 V, I = 140 pA). (b) 25 nm<sup>2</sup> (U = 1.4 V, I = 140 pA). (c) 12.5 nm<sup>2</sup> (U = 1.5 V, I = 1.0 nA) with superimposed wireframe model where only the carbon skeleton is shown, see Fig. 1c?.

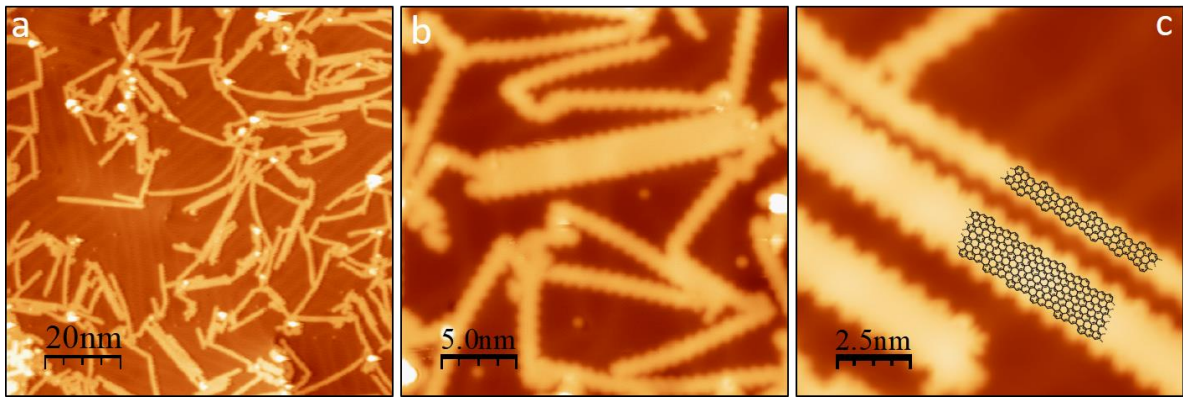


**Figure 3.** Chiral GNRs resulting from TBBA precursor. (a)  $100 \text{ nm}^2$  ( $U = 1.1 \text{ V}$ ,  $I = 80 \text{ pA}$ ). (b)  $25 \text{ nm}^2$  ( $U = 1.0 \text{ V}$ ,  $I = 120 \text{ pA}$ ). (c)  $12.5 \text{ nm}^2$  ( $U = 50 \text{ mV}$ ,  $I = 0.5 \text{ nA}$ ) with superimposed wireframe models showing only the carbon backbone, see Fig. 1e.

After polymerization, intramolecular CDH is induced by annealing the sample to higher temperatures, thereby turning the polymers into planar GNRs. At this point it is easy to identify from the lateral edge morphology that the resulting product is exclusively (3,1)-chGNRs (Fig. 3). This implies a dramatically favored UC via the 2,2' positions between the debrominated precursors, which given the well-known preferred reactivity of acenes at their central ring positions<sup>[19]</sup> is a surprising result. The UC itself being a multistep reaction, the observed preference may arise from any of the different steps. Reactant diffusion can be discarded because it would affect both halogen positions alike. A difference in the barriers associated to the bond formation between two nearby carbon radicals is also unlikely, since they are typically much lower than the barriers associated with the homolytic cleavage of the C-Br bonds<sup>[20]</sup>. Thus, the homolytic cleavage seems to be the determining step.

We have indeed proven the sequential Br activation by temperature-dependent XPS measurements. Fig. 4 (left) depicts the evolution of Br 3d core level spectra in the temperature range that displays the changes. At low temperatures, the spectra shows two different sets of Br 3d doublets (marked with green and red arrows, respectively), each associated with one of the different Br pairs. As the temperature is raised, the doublet at higher binding energies disappears first (green arrows), with a relatively sharp transition temperature around 525 K. We thus associate this Br 3d doublet to the Br at 2,2' positions (green arrows). Subsequently, the second doublet also fades (red arrows), although with a smoother temperature dependence. Concomitant with the disappearance of those two core level doublets, a new one appears at a binding energy more than 2 eV lower, associated with the atomic Br adsorbed on the metal surface (blue arrows). Its intensity profile (Fig. 4, right) as a function of temperature (at ~68.9 eV, see the vertical dashed blue line), reveals two distinct increases that correlate with the activation temperatures of each of the 'organic Br pairs', marked respectively with green and red horizontal lines as a guide to the eye. Finally, at around 615 K the Br 3d core level intensity disappears, indicating the desorption of Br from the surface. Because Br desorbs preferentially as HBr,<sup>[21]</sup> this desorption temperature can be associated with the CDH temperature, at which H becomes available for Br atoms to combine with and desorb. Although the threshold temperature values extracted from the XPS and STM analyses differ, this may relate to the different chambers and temperature measurement methods used

(pyrometer vs. thermocouple, respectively). However, most importantly, their combination unambiguously reveals a stepwise activation of the different Br species within the reactant.

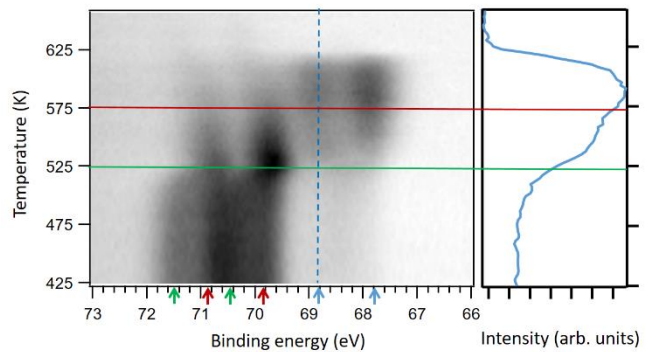


**Figure 4.** Photoemission spectra of the Br 3d core levels of precursor TBBA and their evolution as a function of sample annealing. At the right, an intensity profile at ~68.9 eV (vertical blue dashed line on the left) reveals the two distinct intensity increases with temperature. The different doublet energies for the 2,2' and 10,10' positions, as well as for the detached Br are marked with colored arrows (green, red and blue, respectively) as a guide to the eye.

For a better understanding of the experimental findings we performed DFT calculations on this system. We studied the homolytic cleavage of C-Br bonds in TBBA and dibromoanthracene (DBA) molecules in the gas phase and found that the 10,10' positions exhibit a slightly higher reactivity (i.e., a lower C-Br dissociation binding energy) than the 2,2' positions with a marginal difference of 1.1 kcal/mol for both molecules, suggesting that having an additional neighboring DBA subunit (as in TBBA) has a negligible impact on the dissociation binding energy of C-Br bonds (i.e., DBA and the more sterically congested TBBA have almost identical C-Br dissociation binding energies). The preference for 2,2' positions for TBBA on Au(111) surface must thus have a different origin. To address a possible influence of the substrate, we investigate the relative stability of two adsorption configurations in which the C<sub>2</sub>-Br can be either oriented towards (Fig. 5a) or away from (Fig. 5b) the surface. Both configurations show a dihedral angle between the anthracene subunits of ~127°, consistent with the relatively low energy cost (~5 kcal/mol) needed to distort from the 90° optimum angle calculated for TBBA molecule in gas phase (Fig. S6). We find that

the adsorption geometry with C<sub>2</sub>-Br pointing towards the surface is 8.92 kcal/mol more favorable, making it the dominant configuration on Au(111). Although as deposited molecules are difficult to image experimentally and display notable polymorphism and disorder, the best recognizable structure indeed fits an assembly of molecules with the C<sub>2</sub>-Br pointing down (Fig. S4). Interestingly, in this conformation bromine atoms located at positions 2 and 2' are closer to the surface by ~0.27 Å than those at positions 10 and 10' (Fig. 5a and Fig. S7). A difference that may be further enhanced as the temperature increases, taking into account the vibrational modes of the respective C-Br bonds (with the C<sub>2</sub>-Br bonds pointing towards the surface more than C<sub>10</sub>-Br). As the homolytic cleavage of the C-Br bonds can be catalyzed by metallic substrates<sup>[20]</sup>, we associate this proximity to the substrate with an enhanced catalytic effect on the C<sub>2</sub>-Br bonds, which in turn promotes the polymerization along the 2,2' rather than along the 10,10' positions.

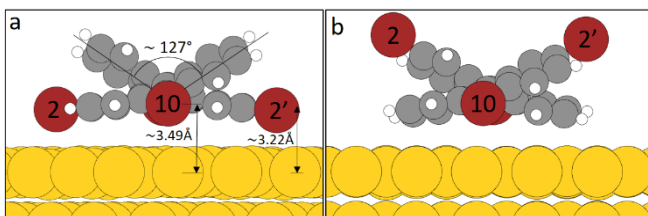


**Figure 5.** Simulated models for the adsorption of TBBA precursor on Au(111). Adsorption configuration with C<sub>2</sub>-Br pointing (a) towards (the global minimum) or (b) away from the surface, 0.387 eV less stable than (a). The yellow, gray, red, and white spheres represent the Au, C, Br, and H atoms, respectively.

Lastly, it is important to note that the chiral ribbons display a variety of widths, which in turn indicates a lateral fusion of the polymers. Although the cyclodehydrogenative fusion of GNRs has been reported earlier and would lead to similar results<sup>[22]</sup>, in this particular case it can be discarded. The reason for this is that while samples prepared from 2,2'-DBBA reveal no lateral fusion of the chiral ribbons after annealing to temperatures of 590 K (Fig. S5a), starting from TBBA at a similar coverage we observe wider, fused GNRs readily at 530 K (Fig. S5b). The additional halogenation thus appears to be an efficient way to increase the chiral ribbons' widths (with its associated impact on their electronic properties<sup>[23]</sup>) with only mild annealing treatments.

Knowing that 530 K is not sufficient to drive the lateral cyclodehydrogenative fusion, the presence of radicals must be involved. It seems unlikely that GNRs would display radicals at the 10,10' positions because they would most probably be immediately saturated by the hydrogen released in intramolecular CDH. We can thus conclude that the lateral fusion must occur in the polymeric phase, when the polymers may still be displaying the radicals at the 10,10' positions and following the alternative coupling direction outlined in Fig. 1c. The fact that most ribbons are only one-monomer wide implies that this lateral coupling is not very effective. This may be ascribed to two different factors that may both contribute, presumably playing together. One is the chiral nature of reactants and polymers, which only allows UC between molecules with the same chirality. The deposited reactants being a racemic mixture, there is a 50% chance for two neighboring polymers to display the same chirality and thereby allow for lateral UC. In addition, the steric hindrance between the

up-pointing anthryl units of neighboring polymers sharing the same chirality may interfere and further limit their coupling.

## Conclusions

In conclusion, we have evaluated the reactivity of multiple C-Br bonds located at different positions within the same aromatic precursor and observed how the relative distance of the halogens with respect to the substrate results in the selective activation at C<sub>2</sub> sites due to the closer proximity to the catalyst. This favored reactivity promotes one of the possible reaction pathways and limits the product formation to chiral GNRs. Particularly interesting is the fact that selective substrate-induced debromination at C<sub>2</sub> position overrules the well-known preferred reactivity of acenes at the central rings (C<sub>10</sub> positions in the case of DBBA precursor). Our results underscore the critical influence of the catalytic substrate on surface-assisted Ullmann coupling. We also demonstrate the use of surface adsorption to design new synthetic strategies that redirect the innate reactivity of aromatic molecules. Specifically, surface adsorption can afford new hierarchical synthetic routes even when carbon atoms are functionalized with the same halogen atoms.

## Experimental Section

### Experimental Methods

Samples were prepared by deposition of 2,2',10,10'-tetrabromo-9,9'-bianthracene (see supporting information for the synthesis of this molecule) precursor from Knudsen cell evaporators heated up to 475 K for sublimation. A single crystal Au(111) surface was used as substrate, prepared by standard sputtering/annealing cycles. STM samples analysis was performed at 4.3 K under ultrahigh vacuum (UHV) at pressures below 10<sup>-10</sup> mbar. All STM images were processed by WSxM software<sup>[24]</sup>.

XPS experiments were performed at the PEARL beamline at the Swiss Light Source (SLS). Samples were prepared using similar conditions to those used for STM experiments. Sample temperatures were calibrated using the readout of two optical pyrometers as a function of sample heating current. The Br 3d signal was monitored during a temperature ramp from RT to 380°C over the course of 8 hours, with each full scan taking approximately 5 minutes (99 scans total). The temperature ramp was performed by incrementally increasing the sample filament current (in direct proximity to the sample) before every scan. A photon energy of 420 eV and an analyser pass energy of 50 eV were used.

### Computational Methods

All gas phase calculations were performed using the program ORCA (version 4.0.1.2)<sup>[25]</sup>. In all calculations we included van der Waals corrections according to the Grimme's D3 approach<sup>[26]</sup> with the Becke-Johnson damping scheme (D3BJ). We used a triple-zeta quality basis set (def2-TZVP)<sup>[27]</sup> and the "TightSCF" keyword for all geometry relaxations. We performed relaxed surface scans to map out the energy profile for the rotation around the single C-C bond connecting the anthracene subunits in TBBA. We also estimated the gas-phase dissociation bond energy for the homolytic cleavage of the C<sub>2</sub>-Br and C<sub>10</sub>-Br bonds in TBBA and in 2,10-dibromoanthracene monomer. The dissociated radical species were calculated at the unrestricted level. Since we are comparing the relative strength between very similar C-Br bonds, zero point energy (ZPE) contributions were not calculated.

For gas-phase calculations, we compared different exchange-correlation functionals, including GGA (PBE)<sup>[30]</sup> and hybrid, namely, PBE0<sup>[28]</sup> and B3LYP<sup>[29]</sup>. We found that PBE provides a good compromise between

accuracy and computational cost for this system and it will be the functional adopted in slab calculations. Finally, since PBE compares well with hybrid functional B3LYP in the energy profile, PBE0 energies were obtained from single point calculations on the PBE-relaxed geometries.

All slab calculations used the PBE exchange-correlation functional<sup>[30]</sup>. Since we are dealing with physisorbed molecules, we included van der Waals (vdW) corrections via the Grimme's D3 method<sup>[26]</sup>. We investigated different adsorption sites of the TBBA molecule (chemical formula C<sub>28</sub>H<sub>14</sub>Br<sub>4</sub>) on the Au(111) surface.

An unreconstructed Au(111) surface was modeled with the coordinates derived from the experimental lattice constant of  $a = 4.0782 \text{ \AA}$ . The low adsorbate coverage limit was investigated using 8x8x4 slabs (256 Au atoms, 64 atoms per layer) that feature lateral adsorbate separations of ~23 Å between the centers of masses. The computational unit cell was [[L, 0.0, 0.0], [L cos( $\pi/3$ ), L sin( $\pi/3$ ), 0.0], [0.0, 0.0, 32.06365]] Å, where  $L=4a\sqrt{2}$ . Only the upper two Au layers are allowed to move during geometry relaxations. An ~18 Å vacuum layer and dipole corrections were used to decouple the periodic images along the normal z direction.

For slab calculations, we used the Quickstep (QS)<sup>[31,32]</sup> module of the CP2K code [version 6.1, revision number: 18464]. QS solves the electronic problem using a hybrid basis set approach that combines Gaussian and plane wave basis sets. The valence Kohn-Sham orbitals were expanded in a double-zeta quality basis set (DZVP-MOLOPT-GTH for the adsorbate, MOLOPT-DZVP-SR-GTH for Au atoms), which is specifically optimized for its use with the GTH pseudopotentials<sup>[33]</sup>. The valence electronic density was expanded using a fully converged plane wave cutoff of 600 Ry. All CP2K calculations were carried out at the converged 3x3x1 K-point sampling and employed an electronic Fermi-Dirac smearing temperature of 300 K. Geometry relaxations were stopped once the maximum ionic force on any atom fell below 1.0e-3 a.u. (0.05 eV/angstrom). Finally, we double-checked our slab CP2K calculations with the code GPAW<sup>[34]</sup> and found consistent results.

## Acknowledgements

The project leading to this publication has received funding from the European Research Council (ERC) under the European Union's Horizon 2020 research and innovation programme (grant agreement No 635919), from the Spanish Ministry of Economy, Industry and Competitiveness (MINECO, Grant Nos. MAT2016-78293-C6-R), We also acknowledge financial support from the Xunta de Galicia (Centro singular de investigación de Galicia, accreditation 2016–2019, ED431G/09) and Fondo Europeo de Desarrollo Regional (FEDER). This work used the "Imbabura" computer cluster of Yachay Tech University, which was purchased under contract No. 2017-024 (SIE-UITEY-007-2017). A.P.P. thanks D.J. Mowbray for his assistance with the computer cluster. We acknowledge the Paul Scherrer Institut, Villigen, Switzerland for provision of synchrotron radiation beamtime at PEARL beamline and would like to thank N. P. M. Bachellier and M. Muntwiller for assistance. We thank R. Fasel and R. Widmer for provision of substrate and sample holder for the synchrotron experiments.

**Keywords:** Density functional calculations • Graphene nanoribbons • Hierarchical synthesis • Scanning probe microscopy • Ullmann coupling

[1] S. E. Thompson y S. Parthasarathy, *Mater. Today* **2006**, 9, 20-25.

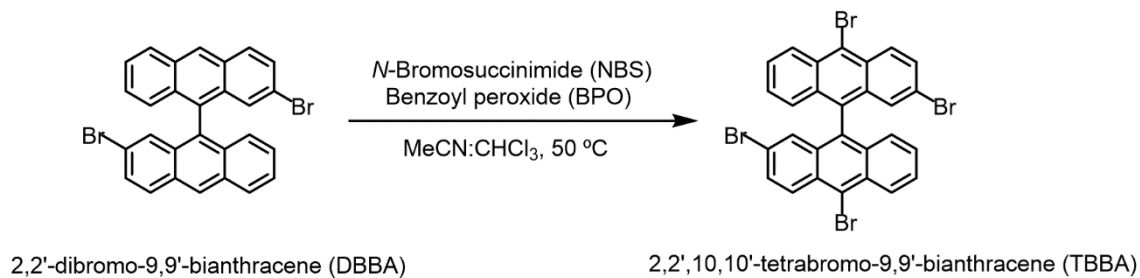
[2] a) A. Gourdon in *On-Surface Synthesis*, Springer International Publishing, Switzerland, **2016**. b) D. G. de Oteyza, C. Rogero in *On-Surface Synthesis II*, Springer International Publishing AG, **2018**. c) S. Clair y D. G. de Oteyza, *Chem. Rev.* **2018**.

- [3] T. Ogawa in *Molecular Electronics*, Springer International Publishing AG, New York, **2017**.
- [4] a) A. Gourdon, *Angew. Chem. Int. Ed.* **2008**, 47, 6950-6953.b) G. Franc y A. Gourdon, *Phys. Chem. Chem. Phys.* **2011**, 13, 14283.
- [5] V. K. Kanuru, G. Kyriakou, S. K. Beaumont, A. C. Papageorgiou, D. J. Watson, y R. M. Lambert, *J. Am. Chem. Soc.* **2010**, 132, 8081-8086.
- [6] S. Weigelt, C. Busse, C. Bombis, M. M. Knudsen, K. V. Gothelf, T. Strunkus, C. Wöll, M. Dahlbom, H. Björk, E. Lægsgaard, F. Besenbacher, T. R. Linderoth, *Angew. Chem. Int. Ed.* **2007**, 46, 9227-9230.
- [7] a) H.-Y. Gao, H. Wagner, D. Zhong, J.-H. Franke, A. Studer, H. Fuchs, *Angew. Chem. Int. Ed.* **2013**, 52, 4024-4028. b) H.-Y. Gao, J.-H. Franke, H. Wagner, D. Zhong, P.-A. Held, A. Studer, H. Fuchs, *J. Phys. Chem. C* **2013**, 117, 18595-18602. c) Y.-Q. Zhang, N. Kepčija, M. Kleinschrodt, K. Diller, S. Fischer, A. Papageorgiou, F. Allegretti, J. Björk, S. Klyatskaya, F. Klappenberger, M. Ruben, J. V. Barth, *Nat. Commun.* **2012**.
- [8] a) D. Zhong, J.-H. Franke, S. K. Podiyannachari, T. Blomker, H. Zhang, G. Kehr, G. Erker, H. Fuchs, I. Chi, *Science* **2011**, 213-216. b) G. Otero, G. Biddau, C. Sánchez-Sánchez, R. Caillard, M. F. López, C. Rogero, F. J. Palomares, N. Cabello, M. A. Basanta, J. Ortega, J. Méndez, A. M. Echavarren, R. Pérez, B. Gómez-Lor, J. A. Martín-Gago, *Nature* **2008**, 454, 865-868. c) F. Bebensee, C. Bombis, S.-R. Vadapoo, J. R. Cramer, F. Besenbacher, K. V. Gothelf, T. R. Linderoth, *J. Am. Chem. Soc.* **2013**, 135, 2136-2139. d) N. A. A. Zwanenveld, R. Pawlak, M. Abel, D. Catalin, D. Gigmes, D. Bertin, L. Porte, *J. Am. Chem. Soc.* **2008**, 130, 6678-6679. e) M. Abel, S. Clair, O. Ourdjini, M. Mossoyan, L. Porte, *J. Am. Chem. Soc.* **2011**, 133, 1203-1205. f) M. Treier, N. V. Richardson, R. Fasel, *J. Am. Chem. Soc.* **2008**, 130, 14054-14055. g) D. G. de Oteyza, P. Gorman, Y.-C. Chen, S. Wickenburg, A. iss, D. J. Mowbray, G. Etkin, Z. Pedramrazi, H.-Z. Tasi, A. Rubio, M. F. Crommie, *Science* **2013**, 340, 1431-1434. h) M. Di Giovannantonio, G. Contini, *J. Phys. Condens. Matter* **2018**, 30, 093001.
- [9] a) F. Ullman, J. Bielecki, *J. Ber. Dtsch. Chem.* **1901**, 34, 2174. b) M. Xi y B. E. Bent, *Surf. Sci.* **1992**, 278, 19-32. c) M. Xi y B. E. Bent, *J. Am. Chem. Soc.* **1993**, 115, 7426-7433. d) S.-W. Hla, L. Bartels, G. Meyer, K.-H. Rieder, *Phys. Rev. Lett.* **2000**, 85, 2777.
- [10] L. Grill, M. Dyer, L. Lafferentz, M. Persson, M. V. Peters, S. Hecht, *Nat. Nanotechnol.* **2007**, 2, 687-691.
- [11] a) M. Di Giovannantonio, M. Tomellini, J. Lipton-Duffin, G. Galeotti, M. Ebrahimi, A. Cossaro, A. Verdini, N. Kharche, V. Meunier, G. Vasseur, Y. Fagot-Revurat, D. F. Parepichka, F. Rosei, G. Contini, *J. Am. Chem. Soc.* **2016**, 138, 16696-16702. b) M. Abadía, M. Illyn, I. Piquero-Zulaica, P. Gargiani, C. Rogero, J. E. Ortega, J. Brede, *ACS Nano* **2017**, 11, 12392-12401. c) C. Bombis, F. Ample, L. Lafferentz, H. Yu, S. Hecht, C. Joachim, L. Grill, *Angew. Chem. Int. Ed.* **2009**, 48, 9966-9970. d) G. Vasseur, Y. Fagot-Revurat, M. Sicot, B. Kierren, L. Moreau, D. Malterre, L. Cardenas, G. Galeotti, J. Lipton-Duffin, F. Rosei, M. Di Giovannantonio, G. Contini, P. Le Fèvre, F. Bertran, L. Liang, V. Meunier, D. F. Perepichka *Nat. Commun.* **2016**, 7, 10235. e) M. Lackinger, *Chem. Commun.* **2017**, 53, 7872-7885. f) M. Kolmer, R. Zuzak, A. K. Steiner, L. Zajac, M. Engelund, S. Godlewski, M. Szymonski, K. Amsharov, *Science* **2019**, 363, 57-60. g) M. Bieri, M.-T. Nguyen, O. Gröning, J. Cai, M. Treier, K. Aït-Mansour, P. Ruffieux, C. A. Pignedoli, D. Passerone, M. Kastler, K. Müllen, R. Fasel, *J. Am. Chem. Soc.* **2010**, 132, 16669-16676. h) R. Gutzler, H. Walch, G. Eder, S. Kloft, W. M. Heckl, y M. Lackinger, *Chem. Commun.* **2009**, 29, 4456.
- [12] C. Pigot, F. Dumur, *Materials* **2019**, 12, 662.
- [13] a) J. Eichhorn, D. Niekarz, O. Ochs, D. Samanta, M. Schmittel, P. J. Szabelski, M. Lackinger, *ACS Nano* **2014**, 8, 7880-7889. b) C. Bronner,

- T. Marangoni, D. J. Rizzo, R. A. Durr, J. H. Jørgensen, F. R. Fischer, M. F. Crommie, *J. Phys. Chem. C* **2017**, 121, 18490-18495. c) M. Di Giovannantonio, J. I. Urgel, R. Widmer, T. Dienel, S. Stoltz, C. Sánchez-Sánchez, M. Muntwiler, T. Dumslaff, R. Berger, A. Narita, X. Feng, K. Müllen, P. Ruffieux, R. Fasel, *ACS Nano* **2017**, 12, 74-81. d) C. Bronner, R. A. Durr, D. J. Rizzo, Y.-L. Lee, T. Marangoni, A. M. Kalayjian, H. Rodriguez, W. Zhao, S. G. Louie, F. R. Fisher, M. F. Crommie, *ACS Nano* **2018**, 12, 2193-2200. e) L. Lafferentz, V. Eberhardt, C. Dri, C. Africh, G. Comelli, F. Esch, S. Hecht, L. Grill, *Nat. Chem.* **2012**, 4, 215-220. f) G. Galeotti, M. Di Giovannantonio, J. Lipton-Duffin, M. Ebrahimi, S. Tebi, A. Verdini, L. Floreano, Y. Fagot-Revurat, D. F. Perepichka, F. Rosei, G. Contini, *Faraday Discuss.* **2017**, 204, 453-469. h) M. Kittelmann, M. Nimmrich, R. Lindner, A. Gourdon, A. Kühnle, *ACS Nano* **2013**, 7, 5614-5620. i) S. Kawai, S. Nakatsuka, T. Hatakeyama, R. Pawlak, T. Meier, J. Travey, E. Meyer, A. S. Foster, *Sci. Adv.* **2018**, 4.
- [14] a) D. G. de Oteyza, A. García-Lekue, M. Vilas-Varela, N. Merino-Díez, E. Carbonell-Sanromà, M. Corso, G. Vasseur, C. Roger, E. Gutián, J. I. Pascual, J. E. Ortega, Y. Wakayama, D. Peña, *ACS Nano* **2016**, 10, 9000-9008. b) J. Cai, P. Ruffieux, R. Jaafar, M. Bieri, T. Braun, S. Blankenburg, M. Muoth, A. P. Seitsonen, M. Saleh, X. Feng, K. Müllen, R. Fasel, *Nature* **2010**, 466, 470. c) P. Han, K. Akagi, F. F. Canova, H. Mutoh, S. Shiraki, K. Iwaya, P. S. Weiss, N. Asao, T. Hitosugi, *ACS Nano* **2014**, 8, 9181-9187.
- [15] a) C. Sánchez-Sánchez, T. Dienel, O. Deniz, P. Ruffieux, R. Berger, X. Feng, K. Müllen, R. Fasel, *ACS Nano* **2016**, 10, 8006-8011. b) F. Schulz, P. H. Jacobse, F. F. Canova, J. van der Lit, D. Z. Gao, A. van der Hoogenband, P. Han, R. J. M. Klein Gebbink, M.-E. Moret, P. M. Joensuu, I. Swart, P. Liljeroth *J. Phys. Chem. C* **2017**, 121, 2896-2904.
- [16] a) V. V. Cherkez, V. V. Zheltov, C. Didiot, B. Kierren, Y. Fagot-Revurat, D. Malterre, B. V. Andryushechkin, G. M. Zhidomirov, K. N. Eltsov, *Phys. Rev. B* **2016**, 93, 045432. b) V. V. Zheltov, V. V. Cherkez, B. V. Andryushechkin, G. M. Zhidomirov, B. Kierren, Y. Fagot-Revurat, D. Malterre, K. N. Eltsov, *Phys. Rev. B* **2015**, 89, 195425.
- [17] M. di Giovannantonio, O. Deniz, Jose I. Urgel, R. Wilmer, T. Dienel, S. Stoltz, C. Sánchez-Sánchez, M. Muntwiler, T. Dumslaff, R. Berger, A. Narita, X. Feng, K. Müllen, P. Ruffieux, R. Fasel, *ACS Nano*, **2017**, 12, 74-81.
- [18] C. Bronner, J. Björk, P. Tegeder, *J. Phys. Chem. C* **2015**, 119, 486-493.
- [19] a) K. Fukui, T. Yonezawa, H. Shingu, *J. Chem. Phys.* **1952**, 20, 5.b) K. Fukui, T. Yonezawa, C. Nagata, H. Shingu, *J. Chem. Phys.* **1954**, 11, 1453. c) S. S. Zade, N. Zamoshchik, A. R. Reddy, G. Fridman-Marueli, D. Sheberla, M. Bendikov, *J. Am. Chem. Soc.* **2011**, 133, 10803-10816. d) S. S. Zade, M. Bendikov, *J. Phys. Org. Chem.* **2012**, 25, 452-461.
- [20] J. Björk, F. Hanke, S. Stafström, *J. Am. Chem. Soc.* **2013**, 135, 5768-5775.
- [21] a) A. Mairena, M. Baljozovic, M. Kawecki, K. Grenader, M. Wienke, K. Martin, L. Bernard, N. Avarvi, A. Terfort, K. H. Ernst, C. Wäckerlin, *Chemical Science* **2019**, 10, 2998-3004. b) C. Bronner, J. Björk, P. Tegeder, *J. Phys. Chem. C.*, **2015**, 1, 486-493.
- [22] a) H. Huang, D. Wei, J. Sun, S. L. Wong, Y. P. Feng, A. H. C. Neto, A. T. S. Wee, *Sci. Rep.* **2012**, 983. b) S. Wang, N. Kharche, E. Costa Girão, X. Feng, K. Müllen, V. Meunier, R. Fasel, P. Ruffieux, *Nano Lett.* **2017**, 17, 4277-4283. c) Z. Chen, H. I. Wang, N. Bilbao, J. Teyssandier, T. Prechtl, N. Cavani, A. Tries, R. Biagi, V. De Renzi, X. Feng, M. Kläui, S. de Feyter, M. Bonn, A. Narita, K. Müllen, *J. Am. Chem. Soc.* **2017**, 139, 9483-9486. d) C. Ma, L. Liang, Z. Xiao, A. A. Puretzky, K. Hong, W. Lu, V. Meunier, J. Bernholc, A.-P. Li, *Nano Lett.* **2017**, 17, 6241-6247. e) O. Deniz, C. Sánchez-Sánchez, T. Dumslaff, X. Feng, A. Narita, K. Müllen, N. Kharche, V. Meunier, R. Fasel, P. Ruffieux, *Nano Lett.* **2017**, 17, 2197-2203. f) A. Basagni, F. Sedona, C. A. Pignedoli, M. Cattelan, L. Nicolas, M. Casarin, M. Sambi. *J. Am. Chem. Soc.* **2015**, 137, 1802-1808. g) N. Merino-Díez, A. García-Lekue, E. Carbonell-Sanromà, J. Li, M. Corso, L. Colazzo, F. Sedona, D. Sánchez-Portal, J. I. Pascual, *ACS Nano* **2017**, 11, 11661-11668. h) N. Merino-Díez, J. Lobo-Checa, P. Nita, A. García-Lekue, A. Basagni, G. Vasseur, F. Tiso, F. Sedona, P. K. Das, J. Fujii, I. Vobornik, M. Sambi, J. I. Pascual, J. E. Ortega, D. G. de Oteyza, *J. Phys. Chem. Lett.* **2018**, 9, 2510-2517.
- [23] Martina Corso, Eduard Carbonell-Sanromà, Dimas G. de Oteyza in *Bottom-Up Fabrication of Atomically Precise Graphene Nanoribbons*, Springer-Cham, **2017**.
- [24] I. Horcas, R. Fernández, J. M. Gómez-Rodríguez, J. Colchero, J. Gómez-Herrero, A. M. Baro, *Rev. Sci. Instrum.* **2007**, 78, 013705.
- [25] F. Neese, *Wiley Interdiscip. Rev. Comput. Mol. Sci.* **2012**, 2, 73-78.
- [26] a) S. Grimme, S. Ehrlich, L. Goerigk, *J. Comput. Chem.* **2011**, 32, 1456-1465. b) S. Grimme, J. Antony, S. Ehrlich, H. Krieg, *J. Chem. Phys.* **2010**, 132, 154104.
- [27] F. Weigend, R. Ahlrichs, *Phys. Chem. Chem. Phys.* **2005**, 7, 3297.
- [28] C. Adamo, V. Barone, *J. Chem. Phys.* **1999**, 110, 6158-6170.
- [29] a) A. D. Becke, *J. Chem. Phys.* **1993**, 98, 5648-5652. b) P. J. Stephens, F. J. Devlin, C. F. Chabalowski, M. J. Frisch, *J. Phys. Chem.* **1994**, 98, 11623-11627.
- [30] J. P. Perdew, K. Burke, M. Ernzerhof, *Phys. Rev. Lett.* **1996**, 77, 3865-3868.
- [31] J. VandeVondele, M. Krack, F. Mohamed, M. Parrinello, T. Chassaing, J. Hutter, *Comput. Phys. Commun.* **2005**, 167, 103-128.
- [32] J. Hutter, M. Iannuzzi, F. Schiffmann, J. VandeVondele, *Wiley Interdiscip. Rev. Comput. Mol. Sci.* **2014**, 4, 15-25.
- [33] S. Goedecker, M. Teter, J. Hutter, *Phys. Rev. B* **1996**, 54, 1703-1710.
- [34] a) J. J. Mortensen, L. B. Hansen, K. W. Jacobsen, *Phys. Rev. B* **2005**, 71, 2005. b) J. Enkovaara, C. Rostgaard, J. J. Mortensen, J. Chen, M. Dulak, L. Ferrighi, J. Gavnholt, C. Glinsvad, V. Haikola, H. A. Hansen, H. H. Kristoffersen, M. Kuusma, A. H. Larsen, L. Lehtovaara, M. Ljungberg, O. Lopez-Acevedo, P. G. Moses, J. Ojanen, T. Olsen, V. Petzold, N. A. Romero, J. Stausholm-Møller, M. Strange, G. A. Tritsaris, M. Vanin, M. Walter, B. Hammer, H. Häkkinen, G. K. Madsen, R. M. Nieminen, J. K. Nørskov, M. Puska, t. T. Rantala, J. Schiøtz, K. S. Thygesen, K. W. Jacobsen, *J. Phys. Condens. Matter* **2010**, 22, 253202.

## Supplementary information

## 1. Synthesis and characterization of TBBA



**Scheme S1.** Synthesis of 2,2',10,10'-tetrabromo-9,9'-bianthracene (TBBA).

N-Bromosuccinimide (NBS, 335 mg, 1.88 mmol) was added over a mixture of 2,2'-dibromo-9,9'-bianthracene<sup>1</sup> (DBBA, 64 mg, 0.12 mmol) and benzoyl peroxide (BPO, 5 mg) dissolved in MeCN:CHCl<sub>3</sub> (1:1, 8 mL). The resulting mixture was heated under argon at 50 °C for 16 h. Then, the reaction mixture was concentrated under reduced pressure and the resulting residue was purified by column chromatography (SiO<sub>2</sub>, hexane/CH<sub>2</sub>Cl<sub>2</sub> 9:1) to afford 2,2',10,10'-tetrabromo-9,9'-bianthracene (TBBA, 80 mg, 95% yield) as a yellow solid (mp: 362 °C).

<sup>1</sup>H NMR (323 K, 500 MHz, CDCl<sub>3</sub>) δ: 8.70 (d, *J* = 8.9 Hz, 2H), 8.61 (d, *J* = 9.4 Hz, 2H), 7.63 (dd, *J* = 9.4, 1.9 Hz, 2H), 7.61 (ddd, *J* = 9.0, 6.5, 1.1 Hz, 2H), 7.23 – 7.20 (m, 4H), 6.99 (d, *J* = 8.8 Hz, 2H) ppm.

<sup>13</sup>C NMR-DEPT (323 K, 125 MHz, CDCl<sub>3</sub>) δ: 133.0 (2C), 132.9 (2C), 131.7 (2C), 131.1 (2CH), 130.9 (2C), 130.4 (2CH), 129.1 (2C), 128.6 (2CH), 128.4 (2CH), 127.9 (2CH), 127.4 (2CH), 127.1 (2CH), 125.0 (2C), 121.8 (2C) ppm.

MS (EI)  $m/z$  (%): 670 ( $M^+$ , 100), 348 (20), 214 (16), 174 (49).

HRMS: C<sub>28</sub>H<sub>14</sub>Br<sub>4</sub>; calculated: 665.7829, found: 665.7830

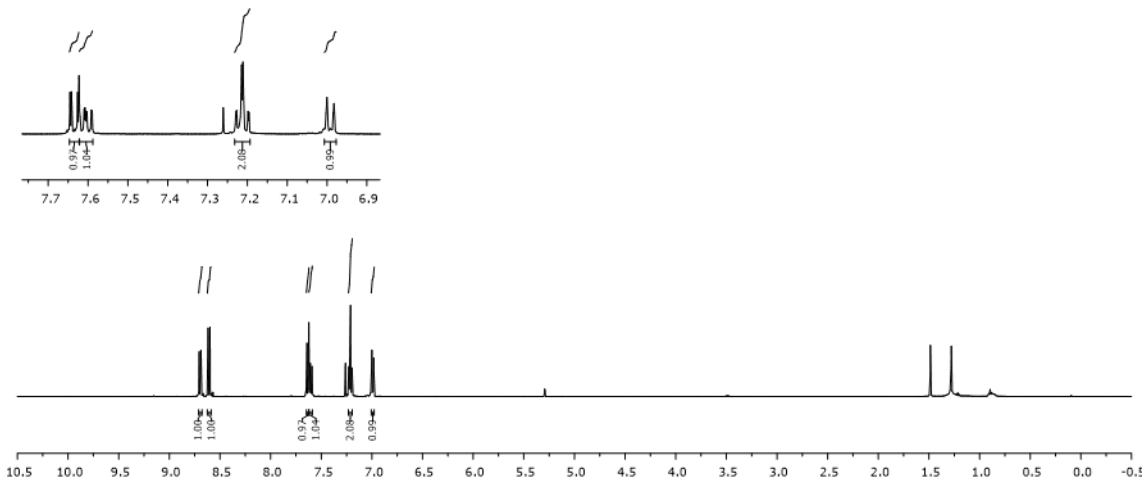


**Figure S1.**  $^1\text{H}$  NMR spectrum of 2,2',10,10'-tetrabromo-9,9'-bianthracene (TBBA)

[1] D. G. de Oteyza, A. García-Lekue, M. Vilas-Varela, N. Merino-Díez, E. Carbonell-Sanromà, M. Corso, G. Vasseur, C. Rogero, E. Gutián, J. I. Pascual, J. E. Ortega, Y. Wakayama, D. Peña, *ACS Nano* **2016**, 10, 9000-9008.

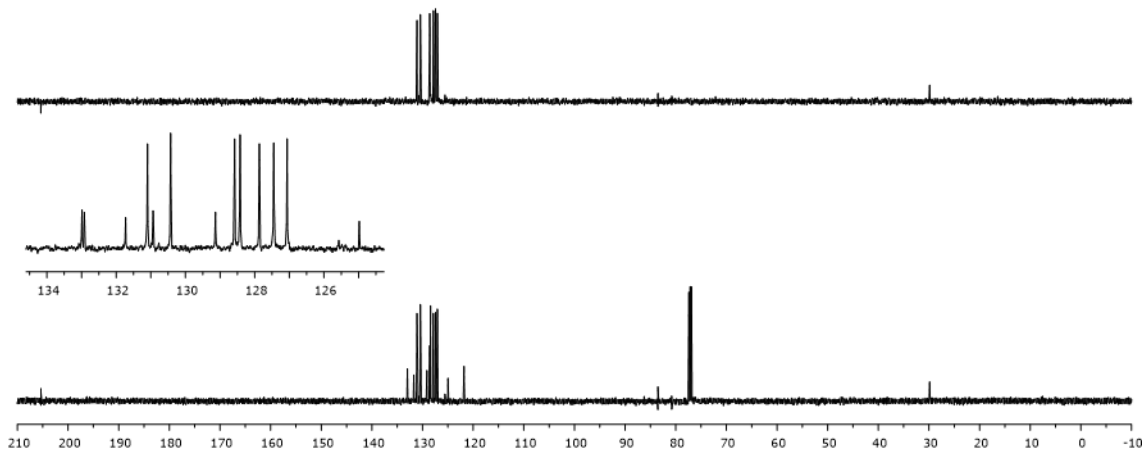


**Figure S2.**  $^{13}\text{C}$  NMR spectrum of 2,2',10,10'-tetrabromo-9,9'-bianthracene (TBBA)

## 2. Additional STM Images

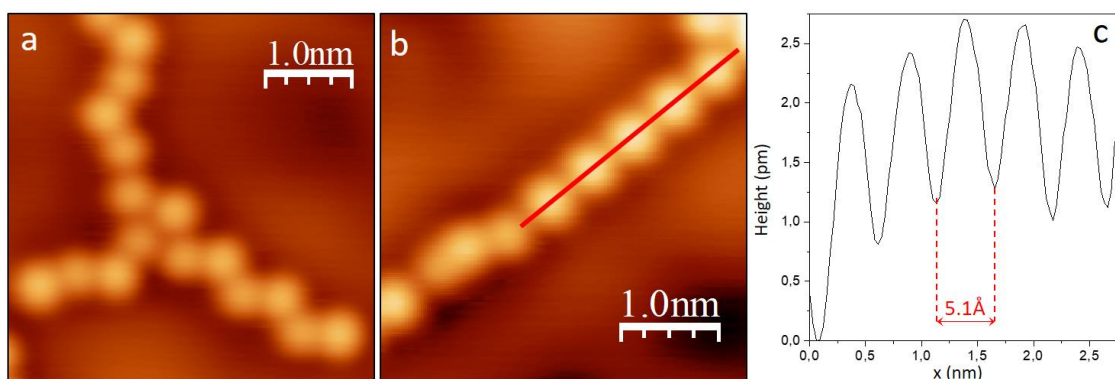


**Fig. S3.** STM images ( $U = 65$  mV,  $I = 250$  pA) showing bromine atoms arranged (a) in zigzag and (b) in line. (c) Line profile corresponding to the red line in (b).

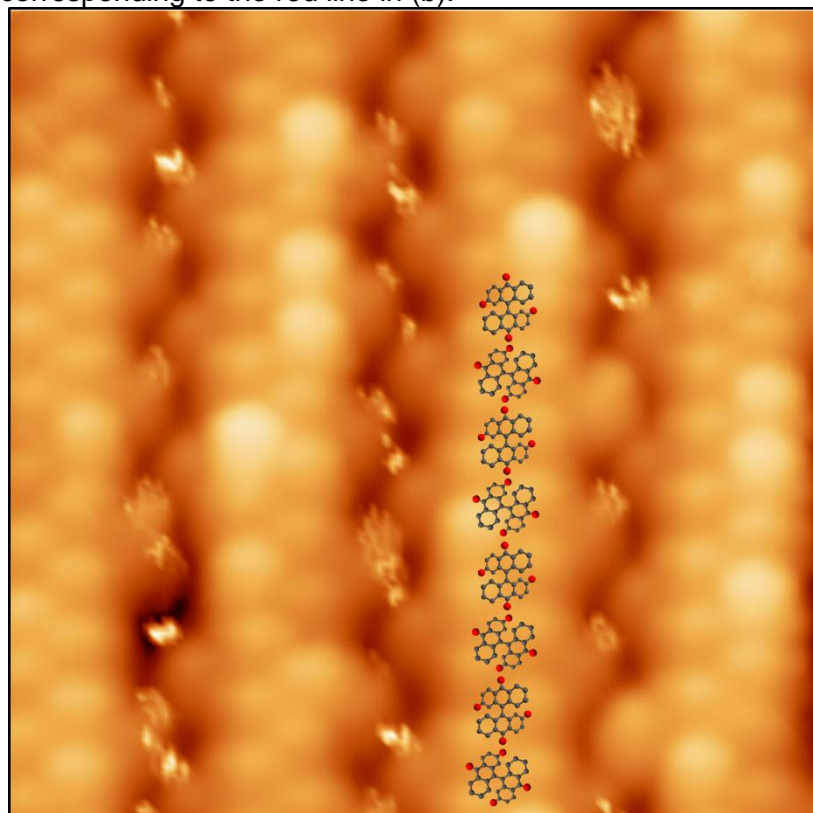


**Fig. S4. As deposited reactant molecules and tentative model of this particular ordered structure.** The molecules display alternating orientation and the structure is presumably stabilized by halogen bonding of the Br atoms along the molecular rows. Only the Br atoms at 10,10' positions and facing out of the molecular rows are observed (every second molecule along the rows), the rest being hidden from the scanning probe by the neighboring up-pointing anthracenes.

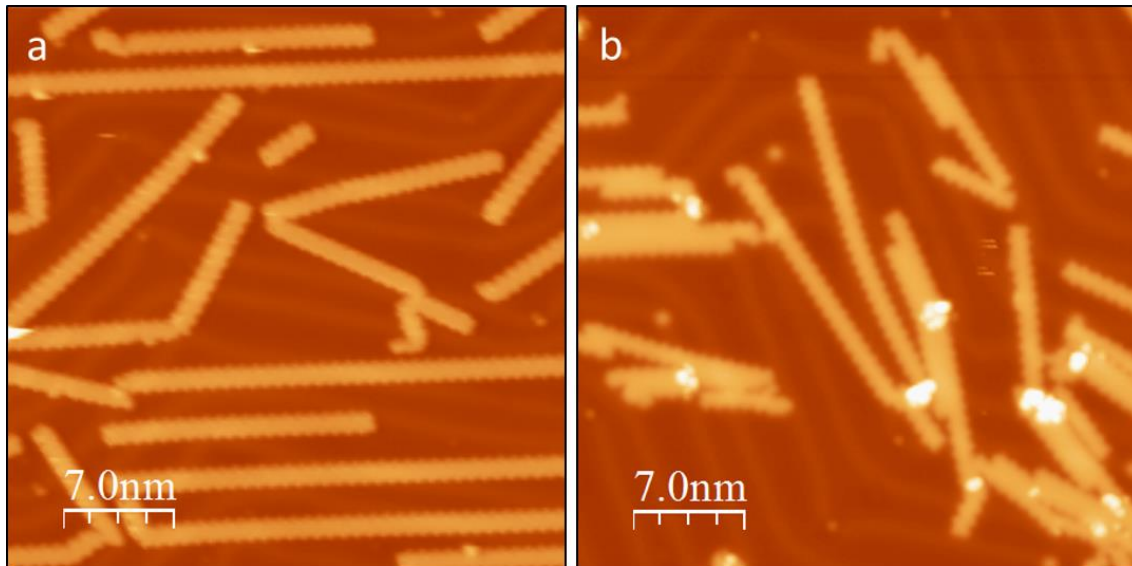


**Fig. S5.** Comparative images of samples obtained with (a) 2,2'-DBBA after annealing to 590 K ( $U = 0.8$  V ,  $I = 20$  pA ) and with (b) TBBA after annealing to only 530 K ( $U = 0.8$  V ,  $I = 50$  pA ).

### 3. Computational calculations

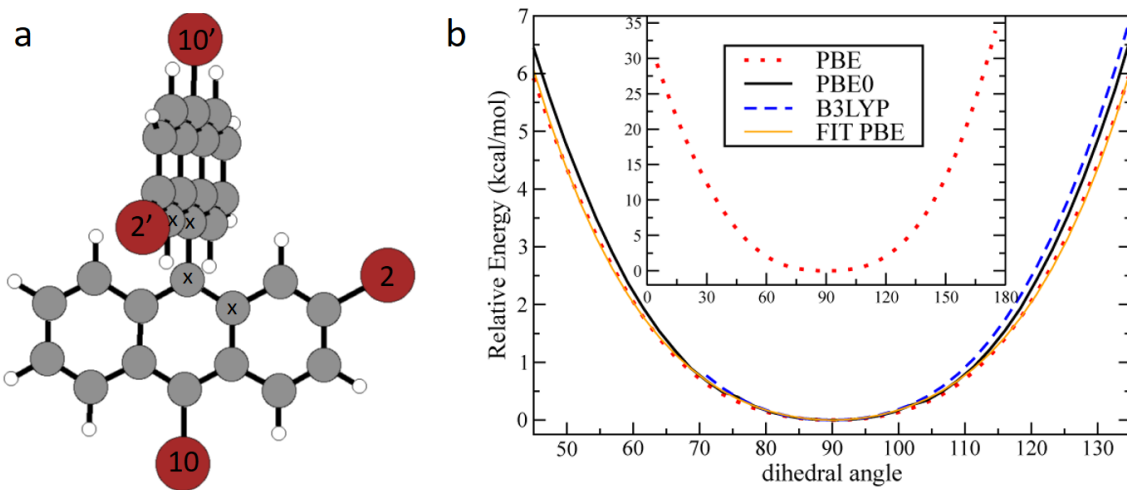


**Fig. S6. Energy cost to rotate anthracene subunits out from the 90° optimum dihedral angle in gas phase.** (a) Relaxed structure of gas-phase TBBA calculated at the PBE-D3/def2-TZVP level. The bromine positions (2, 2', 10, and 10') are indicated. This global minimum conformation features a dihedral angle (defined by the "x" symbols, 0° means eclipsing Br atoms at 2 and 2' positions) of 90°, that is, the two anthracene subunits are perpendicular. The gray, red, and white spheres represent the C, Br, and H atoms, respectively. (b) Calculated energy profile for the rotation around the single C-C bond connecting the anthracene subunits of TBBA in gas phase. Geometries were relaxed at the PBE and B3LYP level with a constraint on the dihedral angle defined in Figure S3a (0° corresponds to eclipsing Br<sub>2</sub> and 2'). PBE0 data are single point energy calculations on the PBE-relaxed geometries. The basis set was def2-TZVP in all cases. The PBE curve can be fitted perfectly (orange line) in the range [45°, 135°] by the following non-linear function:  $V(a)=0.5k_h(a-90)^2+0.25k_q(a-90)^4$ , where  $a$  is the dihedral angle, and the fitted values are  $k_h=0.00334$  and  $k_q=2.621e-6$  kcal/mol for the harmonic and quartic force constants, respectively. The harmonic part alone (not shown) does already an excellent job in the range [70°, 110°] around global minimum. Outside this interval, however, the quartic potential is needed to

accurately describe the full potential. Asymmetry becomes evident at the endpoints (inset shows PBE data on the full range) due to the different steric clashes between approaching phenyl rings. At these endpoints, the flanking phenyl rings distort significantly to reduce steric hindrance.

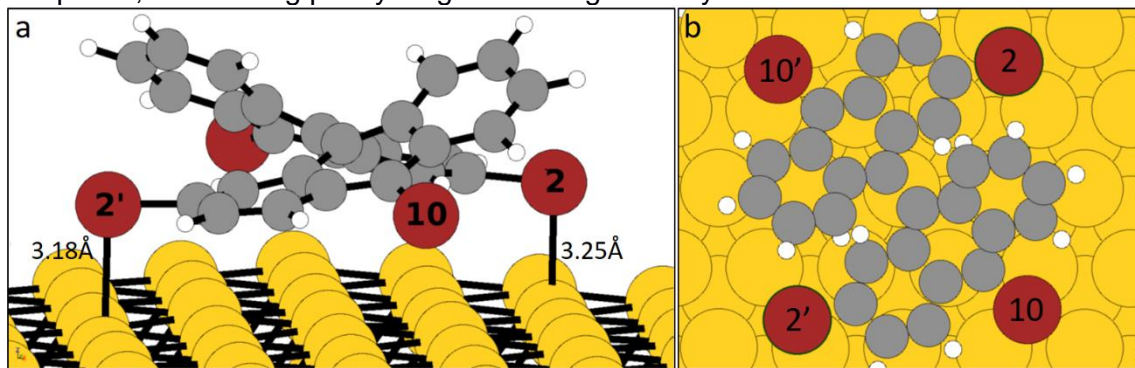


**Fig. S7. Calculated most stable TBBA adsorption configuration.** (a) Side and (b) top views of the calculated most stable adsorption conformation of TBBA on Au(111). All Br atoms are found nearly on bridge positions. The yellow, gray, red, and white spheres represent the Au, C, Br, and H atoms, respectively.

**Supplementary data 1. Relaxed XYZ coordinates from DFT calculations:** a) gas-phase TBBA structure (Fig. S3a) relaxed at the PBE-D3/def2-TZVP level using the ORCA code, (b) adsorption configuration with C<sub>2</sub>-Br pointing away from the surface (Fig. 4b) and (c) detailed adsorption configuration with C<sub>2</sub>-Br pointing towards the surface (global minimum, Fig. S4). The b) and c) structures were relaxed at the PBE-D3 level with the CP2K code.

**a) Gas-phase TBBA structure (Fig. S6a): the total energy is E=-11369.634176 Hartrees computed at the PBE-D3/def2-TZVP level with the ORCA program.**

C	1.325240	2.736104	-3.872177
C	1.270126	1.318097	-3.851679
C	0.785657	0.663786	-2.747356
C	0.328583	1.379464	-1.599203
C	0.894763	3.465797	-2.791841
C	0.383781	2.828236	-1.622673
C	-0.165815	0.700643	-0.466267
C	-0.613241	1.428727	0.655509
C	-0.070476	3.527758	-0.487973
C	-0.569214	2.877232	0.655091
C	-1.116898	0.756645	1.810171
C	-1.550115	1.471749	2.895051
C	-1.512566	2.889928	2.910912
C	-1.033353	3.563663	1.816520
H	1.712608	3.250168	-4.753101
H	1.614259	0.749284	-4.716696
H	0.739966	-0.425615	-2.727030
H	0.939000	4.554210	-2.812154
Br	-0.007616	5.441335	-0.500707
H	-1.151658	-0.332010	1.812979
Br	-2.222036	0.565169	4.428936
H	-1.862539	3.431378	3.789097
H	-1.002129	4.652732	1.826117
C	-3.677364	-2.821660	-1.797663
C	-3.623032	-1.403698	-1.820697
C	-2.498461	-0.750443	-1.383711
C	-1.362348	-1.467230	-0.899010
C	-2.608967	-3.552342	-1.339966
C	-1.419554	-2.915981	-0.876580
C	-0.210393	-0.789735	-0.448641

C	0.898236	-1.518985	0.028524
C	-0.297031	-3.616677	-0.394754
C	0.864469	-2.967414	0.061083
C	2.071541	-0.847983	0.488494
C	3.142729	-1.564032	0.953127
C	3.125109	-2.982162	0.992670
C	2.012533	-3.654927	0.555893
H	-4.575160	-3.334817	-2.145369
H	-4.478805	-0.833911	-2.185729
H	-2.452736	0.339011	-1.398842
H	-2.655637	-4.640709	-1.322656
Br	-0.353483	-5.530164	-0.357324
H	2.099975	0.240620	0.462785
Br	4.702434	-0.659328	1.565379
H	3.992070	-3.524394	1.368499
H	1.996045	-4.743960	0.585415

**b)** Adsorption configuration with C<sub>2</sub>-Br pointing away from the surface (Fig. 5b). The calculated total energy of this configuration is -8735.9943897 Hartrees.

Au	0.0000000000	0.0000000000	9.2134497000
Au	2.8837228800	0.0000000000	9.2134497000
Au	5.7674457500	0.0000000000	9.2134497000
Au	8.6511686300	0.0000000000	9.2134497000
Au	11.5348915000	0.0000000000	9.2134497000
Au	14.4186143800	0.0000000000	9.2134497000
Au	17.3023372500	0.0000000000	9.2134497000
Au	20.1860601300	0.0000000000	9.2134497000
Au	1.4418614400	2.4973772700	9.2134497000
Au	4.3255843100	2.4973772700	9.2134497000
Au	7.2093071900	2.4973772700	9.2134497000
Au	10.0930300600	2.4973772700	9.2134497000
Au	12.9767529400	2.4973772700	9.2134497000
Au	15.8604758100	2.4973772700	9.2134497000
Au	18.7441986900	2.4973772700	9.2134497000
Au	21.6279215600	2.4973772700	9.2134497000
Au	2.8837228800	4.9947545300	9.2134497000
Au	5.7674457500	4.9947545300	9.2134497000
Au	8.6511686300	4.9947545300	9.2134497000
Au	11.5348915000	4.9947545300	9.2134497000
Au	14.4186143800	4.9947545300	9.2134497000
Au	17.3023372500	4.9947545300	9.2134497000
Au	20.1860601300	4.9947545300	9.2134497000
Au	23.0697830000	4.9947545300	9.2134497000
Au	4.3255843100	7.4921318000	9.2134497000
Au	7.2093071900	7.4921318000	9.2134497000
Au	10.0930300600	7.4921318000	9.2134497000
Au	12.9767529400	7.4921318000	9.2134497000
Au	15.8604758100	7.4921318000	9.2134497000
Au	18.7441986900	7.4921318000	9.2134497000
Au	21.6279215600	7.4921318000	9.2134497000
Au	24.5116444400	7.4921318000	9.2134497000
Au	5.7674457500	9.9895090700	9.2134497000
Au	8.6511686300	9.9895090700	9.2134497000
Au	11.5348915000	9.9895090700	9.2134497000
Au	14.4186143800	9.9895090700	9.2134497000
Au	17.3023372500	9.9895090700	9.2134497000
Au	20.1860601300	9.9895090700	9.2134497000

Au	23.0697830000	9.9895090700	9.2134497000
Au	25.9535058800	9.9895090700	9.2134497000
Au	7.2093071900	12.4868863400	9.2134497000
Au	10.0930300600	12.4868863400	9.2134497000
Au	12.9767529400	12.4868863400	9.2134497000
Au	15.8604758100	12.4868863400	9.2134497000
Au	18.7441986900	12.4868863400	9.2134497000
Au	21.6279215600	12.4868863400	9.2134497000
Au	24.5116444400	12.4868863400	9.2134497000
Au	27.3953673100	12.4868863400	9.2134497000
Au	8.6511686300	14.9842636000	9.2134497000
Au	11.5348915000	14.9842636000	9.2134497000
Au	14.4186143800	14.9842636000	9.2134497000
Au	17.3023372500	14.9842636000	9.2134497000
Au	20.1860601300	14.9842636000	9.2134497000
Au	23.0697830000	14.9842636000	9.2134497000
Au	25.9535058800	14.9842636000	9.2134497000
Au	28.8372287500	14.9842636000	9.2134497000
Au	10.0930300600	17.4816408700	9.2134497000
Au	12.9767529400	17.4816408700	9.2134497000
Au	15.8604758100	17.4816408700	9.2134497000
Au	18.7441986900	17.4816408700	9.2134497000
Au	21.6279215600	17.4816408700	9.2134497000
Au	24.5116444400	17.4816408700	9.2134497000
Au	27.3953673100	17.4816408700	9.2134497000
Au	30.2790901900	17.4816408700	9.2134497000
Au	1.4418614400	0.8324590900	11.5679995600
Au	4.3255843100	0.8324590900	11.5679995600
Au	7.2093071900	0.8324590900	11.5679995600
Au	10.0930300600	0.8324590900	11.5679995600
Au	12.9767529400	0.8324590900	11.5679995600
Au	15.8604758100	0.8324590900	11.5679995600
Au	18.7441986900	0.8324590900	11.5679995600
Au	21.6279215600	0.8324590900	11.5679995600
Au	2.8837228800	3.3298363600	11.5679995600
Au	5.7674457500	3.3298363600	11.5679995600
Au	8.6511686300	3.3298363600	11.5679995600
Au	11.5348915000	3.3298363600	11.5679995600
Au	14.4186143800	3.3298363600	11.5679995600
Au	17.3023372500	3.3298363600	11.5679995600
Au	20.1860601300	3.3298363600	11.5679995600
Au	23.0697830000	3.3298363600	11.5679995600
Au	4.3255843100	5.8272136200	11.5679995600
Au	7.2093071900	5.8272136200	11.5679995600
Au	10.0930300600	5.8272136200	11.5679995600
Au	12.9767529400	5.8272136200	11.5679995600
Au	15.8604758100	5.8272136200	11.5679995600
Au	18.7441986900	5.8272136200	11.5679995600
Au	21.6279215600	5.8272136200	11.5679995600
Au	24.5116444400	5.8272136200	11.5679995600
Au	5.7674457500	8.3245908900	11.5679995600
Au	8.6511686300	8.3245908900	11.5679995600
Au	11.5348915000	8.3245908900	11.5679995600
Au	14.4186143800	8.3245908900	11.5679995600
Au	17.3023372500	8.3245908900	11.5679995600
Au	20.1860601300	8.3245908900	11.5679995600
Au	23.0697830000	8.3245908900	11.5679995600

Au	25.9535058800	8.3245908900	11.5679995600
Au	7.2093071900	10.8219681600	11.5679995600
Au	10.0930300600	10.8219681600	11.5679995600
Au	12.9767529400	10.8219681600	11.5679995600
Au	15.8604758100	10.8219681600	11.5679995600
Au	18.7441986900	10.8219681600	11.5679995600
Au	21.6279215600	10.8219681600	11.5679995600
Au	24.5116444400	10.8219681600	11.5679995600
Au	27.3953673100	10.8219681600	11.5679995600
Au	8.6511686300	13.3193454300	11.5679995600
Au	11.5348915000	13.3193454300	11.5679995600
Au	14.4186143800	13.3193454300	11.5679995600
Au	17.3023372500	13.3193454300	11.5679995600
Au	20.1860601300	13.3193454300	11.5679995600
Au	23.0697830000	13.3193454300	11.5679995600
Au	25.9535058800	13.3193454300	11.5679995600
Au	28.8372287500	13.3193454300	11.5679995600
Au	10.0930300600	15.8167226900	11.5679995600
Au	12.9767529400	15.8167226900	11.5679995600
Au	15.8604758100	15.8167226900	11.5679995600
Au	18.7441986900	15.8167226900	11.5679995600
Au	21.6279215600	15.8167226900	11.5679995600
Au	24.5116444400	15.8167226900	11.5679995600
Au	27.3953673100	15.8167226900	11.5679995600
Au	30.2790901900	15.8167226900	11.5679995600
Au	11.5348915000	18.3140999600	11.5679995600
Au	14.4186143800	18.3140999600	11.5679995600
Au	17.3023372500	18.3140999600	11.5679995600
Au	20.1860601300	18.3140999600	11.5679995600
Au	23.0697830000	18.3140999600	11.5679995600
Au	25.9535058800	18.3140999600	11.5679995600
Au	28.8372287500	18.3140999600	11.5679995600
Au	31.7209516300	18.3140999600	11.5679995600
Au	-0.0076251868	1.6597136165	14.0337474118
Au	2.8772273929	1.6576271885	14.0334764794
Au	5.7610766739	1.6564088413	14.0353806378
Au	8.6454657610	1.6568538066	14.0359880371
Au	11.5306313861	1.6588973485	14.0352924969
Au	14.4178230162	1.6596395564	14.0414786722
Au	17.2988832214	1.6616067113	14.0428582843
Au	20.1785538359	1.6620341212	14.0360487157
Au	1.4350252443	4.1548598556	14.0340759500
Au	4.3179970953	4.1556939437	14.0345557105
Au	7.1976180641	4.1521279497	14.0346506393
Au	10.0811304729	4.1515838106	14.0223393321
Au	12.9796153101	4.1509987328	14.0231642474
Au	15.8653423200	4.1540598392	14.0433711647
Au	18.7390234016	4.1589569211	14.0496051027
Au	21.6191628110	4.1572019870	14.0396351721
Au	2.8786046338	6.6537767853	14.0350701985
Au	5.7590109149	6.6551119482	14.0367330794
Au	8.6343697018	6.6499130299	14.0119123882
Au	11.5323980929	6.6568681993	14.0134477446
Au	14.4170850238	6.6539068505	14.0364511762
Au	17.2929161386	6.6479363802	14.0400431227
Au	20.1824571836	6.6492666203	14.0354213918
Au	23.0675564673	6.6490629773	14.0353831030

Au	4.3225171322	9.1529111068	14.0354266937
Au	7.2048513015	9.1549532425	14.0366694251
Au	10.0864342908	9.1678352409	14.0162471608
Au	12.9697967478	9.1644843267	14.0318560988
Au	15.8435899392	9.1475576736	14.0338347451
Au	18.7315280582	9.1414440706	14.0121523324
Au	21.6349763043	9.1425088738	14.0126078987
Au	24.5118693467	9.1509203532	14.0363197226
Au	5.7634908080	11.6510407908	14.0342515367
Au	8.6465854405	11.6570023354	14.0398850173
Au	11.5300611883	11.6650085054	14.0370835876
Au	14.4065223525	11.6539548532	14.0392444801
Au	17.2932352536	11.6481660763	14.0298269887
Au	20.1823317763	11.6549035150	14.0136187043
Au	23.0679360156	11.6485153942	14.0318379124
Au	25.9495202797	11.6498959981	14.0350919598
Au	7.2037985517	14.1497467708	14.0340635507
Au	10.0886997019	14.1508258143	14.0403964988
Au	12.9726489631	14.1483260569	14.0493593890
Au	15.8542819757	14.1495872054	14.0387316896
Au	18.7373203014	14.1551159630	14.0298035396
Au	21.6234852719	14.1520657534	14.0341969631
Au	24.5054720206	14.1472045950	14.0358984214
Au	27.3895568008	14.1475818912	14.0327707322
Au	8.6455428276	16.6457776492	14.0340079443
Au	11.5303020481	16.6433905387	14.0374683188
Au	14.4134625851	16.6433171405	14.0398304936
Au	17.2959673683	16.6461670825	14.0370707039
Au	20.1810614495	16.6465922448	14.0357819640
Au	23.0651333838	16.6460389158	14.0355532327
Au	25.9476138542	16.6456610471	14.0336085603
Au	28.8308881303	16.6461692835	14.0329905755
Au	10.0863419844	19.1420446457	14.0336304319
Au	12.9709192393	19.1392904993	14.0340665637
Au	15.8544073894	19.1396861954	14.0343472187
Au	18.7393308408	19.1396026767	14.0360822685
Au	21.6246297506	19.1423953016	14.0361518084
Au	24.5080352973	19.1439993043	14.0355640652
Au	27.3902466592	19.1434433952	14.0366923652
Au	30.2722179281	19.1441251766	14.0344519359
Au	-0.0114168830	-0.0148259933	16.5706700700
Au	2.8724554433	-0.0158904883	16.5732296388
Au	5.7544355792	-0.0152614567	16.5747009537
Au	8.6363727894	-0.0142382916	16.5763917668
Au	11.5201966698	-0.0123979007	16.5808829128
Au	14.4042116101	-0.0111637589	16.5889327495
Au	17.2871685627	-0.0094674925	16.5861421270
Au	20.1718727072	-0.0111553098	16.5738683657
Au	1.4297774754	2.4822762616	16.5719987414
Au	4.3135891472	2.4836072744	16.5720986722
Au	7.1972829380	2.4854610197	16.5777657648
Au	10.0785958162	2.4829064863	16.5855126770
Au	12.9627965498	2.4800925561	16.5835473525
Au	15.8455632811	2.4836025738	16.5906028427
Au	18.7274933893	2.4853894478	16.5950351585
Au	21.6145562064	2.4813720884	16.5777566062
Au	2.8691948289	4.9815377694	16.5729872754

Au	5.7532554342	4.9830256043	16.5763717287
Au	8.6363913954	4.9852388153	16.5703483156
Au	11.5206911719	4.9753361068	16.4947003149
Au	14.4068689099	4.9781971786	16.5518549531
Au	17.2868346191	4.9770788892	16.6326356630
Au	20.1719312264	4.9713290091	16.6070807938
Au	23.0556100021	4.9781936214	16.5789925969
Au	4.3069975274	7.4809390788	16.5765080527
Au	7.1857878419	7.4837137124	16.5806878877
Au	10.0555754196	7.4942798174	16.4720243482
Au	12.9687499012	7.5046727671	16.5094887801
Au	15.8453009352	7.4652078503	16.6118722938
Au	18.7289017916	7.4521032340	16.5670667873
Au	21.6121606095	7.4695594704	16.5814267434
Au	24.4937692145	7.4785865997	16.5769514386
Au	5.7496538299	9.9816396810	16.5751584810
Au	8.6305845058	9.9892279485	16.5858568705
Au	11.5137008532	9.9993688042	16.5625704476
Au	14.4081631438	9.9880691884	16.6106669539
Au	17.2764824970	9.9481522774	16.5180517994
Au	20.1803741551	9.9637713659	16.4572636850
Au	23.0553023951	9.9752057194	16.5793843806
Au	25.9366281904	9.9783380013	16.5772412705
Au	7.1930223410	12.4811818153	16.5768620396
Au	10.0775395105	12.4847274192	16.6009586456
Au	12.9625798412	12.4737440563	16.6295776779
Au	15.8416493137	12.4670263025	16.5582007859
Au	18.7252186847	12.4783712563	16.5185732082
Au	21.6153366707	12.4749787952	16.5635667419
Au	24.4961053503	12.4750521972	16.5767581686
Au	27.3792484469	12.4779775406	16.5728454737
Au	8.6370481773	14.9768476052	16.5771972861
Au	11.5225407327	14.9704345277	16.5958872723
Au	14.4002498843	14.9678957977	16.5833240290
Au	17.2859259775	14.9705798200	16.5862216836
Au	20.1710096216	14.9710940087	16.5890040511
Au	23.0534806965	14.9726646456	16.5795803671
Au	25.9376938692	14.9745522245	16.5716168322
Au	28.8217747147	14.9766079244	16.5715170329
Au	10.0815204490	17.4695748848	16.5732698077
Au	12.9653116437	17.4660120288	16.5837307512
Au	15.8469826371	17.4641267338	16.5857278182
Au	18.7284901471	17.4649633198	16.5839888550
Au	21.6116532115	17.4687363286	16.5764067487
Au	24.4961611227	17.4712823349	16.5733672266
Au	27.3802393801	17.4729349983	16.5736939953
Au	30.2649355650	17.4733092707	16.5710053328
Br	15.6307791729	3.2893202617	19.9819460921
Br	10.8129891889	9.5497096251	23.2819903412
Br	19.8037738754	8.0855152031	23.5618214417
Br	15.2656383681	14.2295525974	19.9041825896
C	15.3516010593	12.3385686200	20.2761281512
C	14.3289014486	10.2731065888	21.1027413831
C	15.4079124712	9.5052283426	20.5779148245
C	16.5518456860	11.6530660748	20.0073487277
C	12.0171915237	11.7430151362	21.8659423550
C	16.5304460761	10.1998756278	20.0440832793

C	17.7138772844	9.5297727909	19.5926706855
C	18.9014324674	10.2068599359	19.4150522671
C	18.9490044539	11.6194154393	19.5272024363
C	13.3028882514	9.6732394414	21.8932648209
C	12.1888404913	10.3889936648	22.2528429683
C	14.2301056648	11.6946027595	20.8268822118
C	17.7860799119	12.3230063518	19.7466371954
C	11.8958522960	5.8126078587	19.5054672591
C	15.4836796571	5.1746361832	20.3559024489
C	11.9238980661	7.2230604909	19.3558637673
C	13.0950763933	7.9270138844	19.5492796342
C	14.2767753580	7.2875997745	20.0458599467
C	13.0665913559	5.1355160804	19.7583863982
C	14.2813851425	5.8336455880	20.0362600540
C	15.3688368179	8.0112301296	20.6024828550
C	16.4300908571	7.2699393642	21.1985764810
C	13.0260700946	12.3747657585	21.1828522362
C	17.4052841051	7.9023861079	22.0263449587
C	18.5020002505	7.2076119474	22.4708523176
C	18.7076497530	5.8457944458	22.1312329603
C	17.7497806630	5.1873113231	21.4014863185
C	16.5623736137	5.8449531294	20.9586207648
H	17.8035667669	13.4110960109	19.7718845267
H	19.8976454945	12.1449986677	19.4188180954
H	19.8093148712	9.6462854651	19.1858836095
H	17.6999995489	8.4499796487	19.4727177262
H	13.4055341371	8.6325207759	22.1929252764
H	17.87778820747	4.1302415424	21.1739986491
H	19.6022704678	5.3266797196	22.4721831113
H	17.2759136864	8.9495869186	22.2910725945
H	13.0688041044	4.0479249992	19.8072215520
H	13.0902987264	9.0042750494	19.4096493317
H	11.0109814306	7.7629060153	19.1007067734
H	10.9561372210	5.2698974006	19.4001445137
H	11.1072944620	12.2773966820	22.1353659104
H	12.9226706013	13.4265207741	20.9209036062

**c)** Detailed adsorption configuration with C<sub>2</sub>-Br pointing towards from the surface (the global adsorption minimum, Fig. S7). The calculated total energy of this configuration is -8736.008610 Hartrees.

Au 0.00000000 0.00000000 9.21344970  
 Au 2.88372288 0.00000000 9.21344970  
 Au 5.76744575 0.00000000 9.21344970  
 Au 8.65116863 0.00000000 9.21344970  
 Au 11.53489150 0.00000000 9.21344970  
 Au 14.41861438 0.00000000 9.21344970  
 Au 17.30233725 0.00000000 9.21344970  
 Au 20.18606013 0.00000000 9.21344970  
 Au 1.44186144 2.49737727 9.21344970  
 Au 4.32558431 2.49737727 9.21344970  
 Au 7.20930719 2.49737727 9.21344970  
 Au 10.09303006 2.49737727 9.21344970  
 Au 12.97675294 2.49737727 9.21344970  
 Au 15.86047581 2.49737727 9.21344970  
 Au 18.74419869 2.49737727 9.21344970  
 Au 21.62792156 2.49737727 9.21344970  
 Au 2.88372288 4.99475453 9.21344970

Au 5.76744575 4.99475453 9.21344970  
Au 8.65116863 4.99475453 9.21344970  
Au 11.53489150 4.99475453 9.21344970  
Au 14.41861438 4.99475453 9.21344970  
Au 17.30233725 4.99475453 9.21344970  
Au 20.18606013 4.99475453 9.21344970  
Au 23.06978300 4.99475453 9.21344970  
Au 4.32558431 7.49213180 9.21344970  
Au 7.20930719 7.49213180 9.21344970  
Au 10.09303006 7.49213180 9.21344970  
Au 12.97675294 7.49213180 9.21344970  
Au 15.86047581 7.49213180 9.21344970  
Au 18.74419869 7.49213180 9.21344970  
Au 21.62792156 7.49213180 9.21344970  
Au 24.51164444 7.49213180 9.21344970  
Au 5.76744575 9.98950907 9.21344970  
Au 8.65116863 9.98950907 9.21344970  
Au 11.53489150 9.98950907 9.21344970  
Au 14.41861438 9.98950907 9.21344970  
Au 17.30233725 9.98950907 9.21344970  
Au 20.18606013 9.98950907 9.21344970  
Au 23.06978300 9.98950907 9.21344970  
Au 25.95350588 9.98950907 9.21344970  
Au 7.20930719 12.48688634 9.21344970  
Au 10.09303006 12.48688634 9.21344970  
Au 12.97675294 12.48688634 9.21344970  
Au 15.86047581 12.48688634 9.21344970  
Au 18.74419869 12.48688634 9.21344970  
Au 21.62792156 12.48688634 9.21344970  
Au 24.51164444 12.48688634 9.21344970  
Au 27.39536731 12.48688634 9.21344970  
Au 8.65116863 14.98426360 9.21344970  
Au 11.53489150 14.98426360 9.21344970  
Au 14.41861438 14.98426360 9.21344970  
Au 17.30233725 14.98426360 9.21344970  
Au 20.18606013 14.98426360 9.21344970  
Au 23.06978300 14.98426360 9.21344970  
Au 25.95350588 14.98426360 9.21344970  
Au 28.83722875 14.98426360 9.21344970  
Au 10.09303006 17.48164087 9.21344970  
Au 12.97675294 17.48164087 9.21344970  
Au 15.86047581 17.48164087 9.21344970  
Au 18.74419869 17.48164087 9.21344970  
Au 21.62792156 17.48164087 9.21344970  
Au 24.51164444 17.48164087 9.21344970  
Au 27.39536731 17.48164087 9.21344970  
Au 30.27909019 17.48164087 9.21344970  
Au 1.44186144 0.83245909 11.56799956  
Au 4.32558431 0.83245909 11.56799956  
Au 7.20930719 0.83245909 11.56799956  
Au 10.09303006 0.83245909 11.56799956  
Au 12.97675294 0.83245909 11.56799956  
Au 15.86047581 0.83245909 11.56799956  
Au 18.74419869 0.83245909 11.56799956  
Au 21.62792156 0.83245909 11.56799956  
Au 2.88372288 3.32983636 11.56799956  
Au 5.76744575 3.32983636 11.56799956

Au 8.65116863 3.32983636 11.56799956  
Au 11.53489150 3.32983636 11.56799956  
Au 14.41861438 3.32983636 11.56799956  
Au 17.30233725 3.32983636 11.56799956  
Au 20.18606013 3.32983636 11.56799956  
Au 23.06978300 3.32983636 11.56799956  
Au 4.32558431 5.82721362 11.56799956  
Au 7.20930719 5.82721362 11.56799956  
Au 10.09303006 5.82721362 11.56799956  
Au 12.97675294 5.82721362 11.56799956  
Au 15.86047581 5.82721362 11.56799956  
Au 18.74419869 5.82721362 11.56799956  
Au 21.62792156 5.82721362 11.56799956  
Au 24.51164444 5.82721362 11.56799956  
Au 5.76744575 8.32459089 11.56799956  
Au 8.65116863 8.32459089 11.56799956  
Au 11.53489150 8.32459089 11.56799956  
Au 14.41861438 8.32459089 11.56799956  
Au 17.30233725 8.32459089 11.56799956  
Au 20.18606013 8.32459089 11.56799956  
Au 23.06978300 8.32459089 11.56799956  
Au 25.95350588 8.32459089 11.56799956  
Au 7.20930719 10.82196816 11.56799956  
Au 10.09303006 10.82196816 11.56799956  
Au 12.97675294 10.82196816 11.56799956  
Au 15.86047581 10.82196816 11.56799956  
Au 18.74419869 10.82196816 11.56799956  
Au 21.62792156 10.82196816 11.56799956  
Au 24.51164444 10.82196816 11.56799956  
Au 27.39536731 10.82196816 11.56799956  
Au 8.65116863 13.31934543 11.56799956  
Au 11.53489150 13.31934543 11.56799956  
Au 14.41861438 13.31934543 11.56799956  
Au 17.30233725 13.31934543 11.56799956  
Au 20.18606013 13.31934543 11.56799956  
Au 23.06978300 13.31934543 11.56799956  
Au 25.95350588 13.31934543 11.56799956  
Au 28.83722875 13.31934543 11.56799956  
Au 10.09303006 15.81672269 11.56799956  
Au 12.97675294 15.81672269 11.56799956  
Au 15.86047581 15.81672269 11.56799956  
Au 18.74419869 15.81672269 11.56799956  
Au 21.62792156 15.81672269 11.56799956  
Au 24.51164444 15.81672269 11.56799956  
Au 27.39536731 15.81672269 11.56799956  
Au 30.27909019 15.81672269 11.56799956  
Au 11.53489150 18.31409996 11.56799956  
Au 14.41861438 18.31409996 11.56799956  
Au 17.30233725 18.31409996 11.56799956  
Au 20.18606013 18.31409996 11.56799956  
Au 23.06978300 18.31409996 11.56799956  
Au 25.95350588 18.31409996 11.56799956  
Au 28.83722875 18.31409996 11.56799956  
Au 31.72095163 18.31409996 11.56799956  
Au -0.00057997 1.66204397 14.03537198  
Au 2.88233974 1.66322702 14.03518149  
Au 5.76607917 1.66236858 14.03663819

Au 8.65014224 1.65996611 14.03421039  
Au 11.53727716 1.65970157 14.03356056  
Au 14.42479684 1.65945065 14.03561208  
Au 17.30697360 1.66104494 14.03826702  
Au 20.18727040 1.66230420 14.03619625  
Au 1.44152995 4.16066928 14.03378529  
Au 4.32357680 4.16112111 14.03478671  
Au 7.20151327 4.15731926 14.02617459  
Au 10.08486357 4.15534052 14.01537384  
Au 12.98418836 4.15513800 14.01558371  
Au 15.87170843 4.15572649 14.02532673  
Au 18.75101742 4.15949555 14.03411634  
Au 21.63115478 4.15958947 14.03049971  
Au 2.88384596 6.65816158 14.03313961  
Au 5.76785009 6.65927535 14.03505019  
Au 8.64820590 6.66033561 14.02722344  
Au 11.53504590 6.66627033 14.01570537  
Au 14.42746491 6.66248866 14.02115848  
Au 17.30871119 6.66050364 14.03801281  
Au 20.18747918 6.65840677 14.04080548  
Au 23.06935049 6.65738267 14.03482470  
Au 4.32830385 9.15519305 14.03469747  
Au 7.21222147 9.15780861 14.04115621  
Au 10.09307336 9.16758395 14.03808687  
Au 12.97551765 9.17096277 14.03240654  
Au 15.86122650 9.16214902 14.04659566  
Au 18.74497563 9.15395639 14.04914500  
Au 21.62783767 9.15160889 14.04189094  
Au 24.51254195 9.15353963 14.03456738  
Au 5.76829926 11.65208837 14.03585935  
Au 8.64594856 11.65316896 14.04427591  
Au 11.52506749 11.65371327 14.04299582  
Au 14.41051272 11.64503150 14.02281947  
Au 17.30898279 11.64169567 14.02391866  
Au 20.19803689 11.64227797 14.03054944  
Au 23.07536577 11.64831496 14.03600106  
Au 25.95644253 11.65184210 14.03356615  
Au 7.20817563 14.14905056 14.03435085  
Au 10.08825001 14.14943446 14.03791371  
Au 12.97025456 14.14794764 14.02900024  
Au 15.85808269 14.14637066 14.01508807  
Au 18.75458332 14.14470619 14.01491192  
Au 21.63705520 14.14554709 14.02860461  
Au 24.51495407 14.14958725 14.03468764  
Au 27.39762659 14.14981421 14.03379546  
Au 8.65245489 16.64833031 14.03410774  
Au 11.53401367 16.64978274 14.03638206  
Au 14.41656443 16.65345937 14.03031951  
Au 17.30423277 16.65813572 14.01926090  
Au 20.18934059 16.65050970 14.03012427  
Au 23.07190110 16.64721670 14.03455299  
Au 25.95545638 16.64755580 14.03305371  
Au 28.83937811 16.64680601 14.03374894  
Au 10.09382714 19.14375618 14.03622734  
Au 12.97635702 19.14481824 14.03718328  
Au 15.85931168 19.14847479 14.03511141  
Au 18.74582063 19.14838552 14.03515584

Au 21.63043807 19.14440512 14.03751950  
Au 24.51420076 19.14491198 14.03633262  
Au 27.39774617 19.14407995 14.03586864  
Au 30.28060208 19.14331931 14.03591740  
Au 0.00134099 -0.00697120 16.57723661  
Au 2.88397422 -0.00713511 16.57993787  
Au 5.76774506 -0.00645582 16.57987169  
Au 8.65246879 -0.00473443 16.58160994  
Au 11.53873145 -0.00334546 16.57982299  
Au 14.42360678 -0.00254148 16.58149310  
Au 17.30676991 -0.00181007 16.57806010  
Au 20.18914659 -0.00403806 16.57505705  
Au 1.44320598 2.49119846 16.57324012  
Au 4.32668382 2.49120324 16.57390127  
Au 7.20986933 2.49221008 16.57773332  
Au 10.09213753 2.48759368 16.57220861  
Au 12.98358067 2.48926799 16.57792412  
Au 15.86571078 2.49344128 16.59291710  
Au 18.74750460 2.49567471 16.58945716  
Au 21.63039320 2.49206977 16.57827003  
Au 2.88475343 4.98950643 16.57360120  
Au 5.76536299 4.99083011 16.57781785  
Au 8.64157851 4.99224737 16.54346521  
Au 11.53531434 4.97762195 16.46219094  
Au 14.43208074 4.99264247 16.51377312  
Au 17.31015998 4.99001696 16.56057427  
Au 20.19490178 4.98794669 16.57315299  
Au 23.07317068 4.98939147 16.57756141  
Au 4.32681631 7.48911661 16.57304286  
Au 7.20697547 7.49187154 16.58443589  
Au 10.08444442 7.50952475 16.52670633  
Au 12.98852905 7.51468906 16.49678964  
Au 15.87641175 7.49917860 16.56444650  
Au 18.75771147 7.49299768 16.58360409  
Au 21.63537794 7.48582776 16.59133005  
Au 24.51470933 7.48743312 16.57406031  
Au 5.77069876 9.98800321 16.58007050  
Au 8.65145512 9.99176064 16.61845011  
Au 11.53751342 9.98973857 16.64535137  
Au 14.42319758 9.98390212 16.63978221  
Au 17.30729126 9.97523939 16.64338840  
Au 20.19174120 9.97828284 16.61579179  
Au 23.07153131 9.98444692 16.58036407  
Au 25.95590437 9.98609396 16.57144253  
Au 7.20959786 12.48555150 16.59098272  
Au 10.08826276 12.47468306 16.57912238  
Au 12.96965820 12.46926734 16.55726819  
Au 15.85732064 12.45599807 16.49084379  
Au 18.75502577 12.46016480 16.51868944  
Au 21.63249448 12.48113203 16.58158334  
Au 24.51465458 12.48264498 16.57433257  
Au 27.39798839 12.48400582 16.57496856  
Au 8.64736518 14.98207104 16.57366267  
Au 11.53386957 14.98007361 16.56098773  
Au 14.41164140 14.97709088 16.52506552  
Au 17.30532391 14.99305720 16.46846528  
Au 20.20010331 14.98105691 16.54420448

Au 23.07660025 14.98033373 16.57845073  
Au 25.95760163 14.98143411 16.57256539  
Au 28.83904836 14.98123553 16.57842672  
Au 10.09438769 17.47407611 16.58761380  
Au 12.97603086 17.47531535 16.59524510  
Au 15.85802787 17.47836507 16.58290584  
Au 18.74945611 17.48044211 16.57558569  
Au 21.63285501 17.47955999 16.57933585  
Au 24.51581304 17.47910197 16.57268965  
Au 27.39950708 17.47915325 16.57244846  
Au 30.28198964 17.47883050 16.57878835  
Br 18.40341453 6.21211407 19.82818315  
Br 17.78980854 13.93514900 19.50785849  
Br 11.13043482 5.87925123 19.48196732  
Br 10.51054917 13.69289429 19.80957089  
C 11.90102752 12.43715608 20.26062781  
C 14.25542383 11.76042713 20.11268036  
C 13.93371483 10.48151740 20.65423119  
C 11.55140378 11.20822846 20.84844950  
C 14.96917140 14.48628399 19.62157733  
C 12.62414615 10.28922790 21.18013700  
C 12.30899979 9.18560907 22.03131211  
C 11.01517671 8.91063195 22.40311114  
C 9.94953073 9.72093098 21.93123474  
C 15.59174102 12.12647863 19.74415602  
C 15.93428581 13.45115726 19.62253867  
C 13.24080094 12.79718950 20.02247798  
C 10.21263380 10.84588146 21.18844738  
C 18.88438592 10.14532542 22.04759368  
C 16.99312368 7.44074799 20.29093675  
C 17.80321830 10.94924040 22.49422234  
C 16.52116511 10.67240913 22.08500043  
C 16.23310187 9.57171605 21.22070131  
C 18.64669632 9.02712737 21.28633044  
C 17.31941466 8.66296065 20.90552773  
C 14.93612738 9.37390730 20.66570567  
C 14.63339923 8.09394262 20.11655411  
C 13.64376722 14.13985084 19.74862343  
C 13.30453463 7.71381399 19.73475053  
C 12.97928629 6.38541290 19.60892461  
C 13.95639628 5.36194424 19.60500681  
C 15.27681816 5.72408146 19.74245029  
C 15.66054366 7.06904599 20.03099356  
H 9.39998958 11.49695708 20.87033138  
H 8.92005240 9.46699976 22.18577190  
H 10.80425834 8.05963235 23.05152516  
H 13.12323465 8.54687793 22.37272559  
H 16.36076231 11.36609706 19.66929474  
H 16.04749030 4.95669886 19.69530826  
H 13.66931415 4.31820578 19.49074022  
H 12.52666921 8.46476987 19.65900100  
H 19.47031620 8.38128959 20.98620856  
H 15.69551749 11.30547012 22.40904588  
H 17.99301374 11.79617859 23.15437385  
H 19.90505222 10.39884099 22.33586028  
H 15.26958183 15.52686136 19.51296238  
H 12.88300231 14.91701546 19.70169129

